

Observation of SN2011fe with INTEGRAL

I. Pre-maximum phase*

J. Isern¹, P. Jean^{2,3}, E. Bravo⁴, R. Diehl⁵, J. Knödseder^{2,3}, A. Domingo⁶, A. Hirschmann¹, P. Hoefflich⁷, F. Lebrun⁸, M. Renaud⁹, S. Soldi¹⁰, N. Elias-Rosa¹, M. Hernanz¹, B. Kulebi¹, X. Zhang⁵, C. Badenes¹¹, I. Domínguez¹², D. Garcia-Senz⁴, C. Jordi¹³, G. Lichti⁵, G. Vedrenne^{2,3}, and P. Von Ballmoos^{2,3}

(Affiliations can be found after the references)

Received 29 August 2012 / Accepted 13 February 2013

ABSTRACT

Context. SN2011fe was detected by the Palomar Transient Factory in M101 on August 24, 2011, a few hours after the explosion. From the early optical spectra it was immediately realized that it was a Type Ia supernova, thus making this event the brightest one discovered in the past twenty years.

Aims. The distance of the event offered the rare opportunity of performing a detailed observation with the instruments onboard INTEGRAL to detect the γ -ray emission expected from the decay chains of ^{56}Ni . The observations were performed in two runs, one before and around the optical maximum, aimed to detect the early emission from the decay of ^{56}Ni , and another after this maximum aimed to detect the emission of ^{56}Co .

Methods. The observations performed with the instruments onboard INTEGRAL (SPI, IBIS/ISGRI, JEMX, and OMC) were analyzed and compared with the existing models of γ -ray emission from this kind of supernova. In this paper, the analysis of the γ -ray emission has been restricted to the first epoch.

Results. SPI and IBIS/ISGRI only provide upper limits to the expected emission due to the decay of ^{56}Ni . These upper limits on the gamma-ray flux are 7.1×10^{-5} ph/s/cm² for the 158 keV line and 2.3×10^{-4} ph/s/cm² for the 812 keV line. These bounds allow rejecting at the 2σ level explosions involving a massive white dwarf, $\sim 1 M_{\odot}$ in the sub-Chandrasekhar scenario and specifically all models that would have substantial amounts of radioactive ^{56}Ni in the outer layers of the exploding star responsible for the SN2011fe event. The optical light curve obtained with the OMC camera also suggests that SN2011fe was the outcome of the explosion of a CO white dwarf, possibly through the delayed detonation mode, although other ones are possible, of a CO that synthesized $\sim 0.55 M_{\odot}$ of ^{56}Ni . For this specific model, INTEGRAL would have only been able to detect this early γ -ray emission if the supernova had occurred at a distance $\lesssim 2$ Mpc.

Conclusions. The detection of the early γ -ray emission of ^{56}Ni is difficult, and it can only be achieved with INTEGRAL if the distance of the event is close enough. The exact distance depends on the specific SNIa subtype. The broadness and rapid rise of the lines are probably at the origin of this difficulty.

Key words. supernovae: individual: SN2011fe – supernovae: general – gamma rays: stars

1. Introduction

From the photometric point of view, Type Ia supernovae (SNIa) are characterized by a sudden rise and decay in their luminosity, followed by a slowly fading tail. From the spectroscopic point of view, they are characterized by the lack of H-lines and the presence of Si II-lines in their spectra during the maximum light and by the presence of Fe emission features during the nebular phase. A noticeable property is the spectrophotometric homogeneity of the different outbursts. Furthermore, in contrast to the other supernova types, they appear in all kinds of galaxies. These properties point to an exploding object that is compact and free of hydrogen, which can be activated on short and long time scales and is able to synthesize a minimum of $0.3 M_{\odot}$ of radioactive ^{56}Ni to power the light curve. These constraints immediately led to the proposal that SNIa were the outcome of the thermonuclear explosion of a mass-accreting C/O white dwarf (WD) near the Chandrasekhar limit (Hoyle & Fowler 1960) in a close binary system.

* Based on observations with INTEGRAL, an ESA project with instruments and the science data center funded by ESA member states (especially the PI countries: Denmark, France, Germany, Italy, Switzerland, and Spain), the Czech Republic, and Poland and with the participation of Russia and USA.

Despite this homogeneity, some differences appear when SNIa are observed in detail. Now it is known that there is a group of SNIa with light curves showing very bright and broad peaks, the SN1991T class, which represents 9% of all the events. There is another group with a much dimmer and narrower peak and that lacks of the characteristic secondary peak in the infrared, the SN1991bg class, which represents 15% of all the events. To these categories a new one has been recently added that contains very peculiar supernovae: the SN2002cx class, representing $\sim 5\%$ of the total. These supernovae are characterized by high-ionization spectral features in the pre-maximum, such as the SN1991T class, a very low luminosity, and the lack of a secondary maximum in the infrared, as in the SN1991bg class. The remaining ones, which amount to $\sim 70\%$, present normal behavior and are known as *Branch-normal* (Li et al. 2011c). However, even the normal ones are not completely homogeneous, and they show different luminosities at maximum and light curves with different decline rates (Li et al. 2011b). This variety has recently increased with the discovery of SN2001ay, which is characterized by a fast rise and a very slow decline (Baron et al. 2012). This diversity strongly suggests that different scenarios and burning mechanisms could be operating in the explosion.

From the point of view of the explosion mechanism as seen in one-dimensional models, it is possible to distinguish four

cases (Hoefflich & Khokhlov 1996; Hillebrandt & Niemeyer 2000): the pure detonation model (DET), the pure deflagration model (DEF), the delayed detonation model (DDT), and the pulsating detonation model (PDD). The equivalent models in three dimensions also exist, but with a wider variety of possibilities. An additional class are the so-called sub-Chandrasekhar (SCh) models in which a detonation triggered by the ignition of He near the base of a freshly accreted helium layer completely burns the white dwarf. At present, there is no basic argument for rejecting any of the models, except the DET ones that are incompatible with the properties of the spectrum of SNIa at maximum light. Existing observations also pose severe constraints to the total amount of ^{56}Ni that can be produced by the He-layer in SCh models (Hoefflich & Khokhlov 1996; Nugent et al. 1997; Woosley & Kasen 2011).

According to the nature of the companion, either non-degenerate or degenerate, progenitors can be classified as single degenerate systems – SD (Whelan & Iben 1973) – or double degenerate systems – DD (Webbink 1984; Iben & Tutukov 1985). The distinctions are important in order to interpret the observations since, depending on the case, the white dwarf can ignite below, near, or above the Chandrasekhar mass, and consequently the total mass ejected and the mass of ^{56}Ni synthesized can be different. At present, it is not known whether both scenarios can coexist or just one is enough to account for the supernova variety. Observations of the stellar content in the interior of known SNIa remnants point towards one possible SD candidate (Tycho SNR, see Ruiz-Lapuente et al. 2004; González Hernández et al. 2009; Kerzendorf et al. 2009) and two almost certain DD candidates (SNR0509-67.5 and SNR 0519-69.0 Schaefer & Pagnotta 2012; Edwards et al. 2012).

The detection of γ -rays from supernovae can provide important insight into the nature of the progenitor and especially into the explosion mechanism, since the amount and distribution of the radioactive material produced in the explosion strongly depend on how the ignition starts and how the nuclear flame propagates (see Gómez-Gomar et al. 1998; Isern et al. 2008, for a detailed discussion of how these differences are reflected in the spectra). The advantages of using γ -rays for diagnostic purposes relies on their penetrative capabilities, on their ability to distinguish among different isotopes, and on the relative simplicity of their transport modeling as compared with other regions of the electromagnetic spectrum. Unfortunately, such observations have not been achieved so far because of the poor sensitivity of the instruments. For this reason it has only been possible up to now to place upper limits on the SN1991T (Lichti et al. 1994) and SN1998bu (Georgii et al. 2002) events.

Several authors have examined the γ -ray emission from SNIa (Gehrels et al. 1987; Ambwani & Sutherland 1988; Burrows & The 1990; Ruiz-Lapuente et al. 1993; Hoefflich et al. 1994; Kumagai & Nomoto 1997; Timmes & Woosley 1997; Gómez-Gomar et al. 1998; Sim & Mazzali 2008). To explore the above model variants, we used as a guide the properties obtained with the code described in Gómez-Gomar et al. (1998), which is based on the methods described by Pozdnyakov et al. (1983) and Ambwani & Sutherland (1988). To test the consistency of this model, the results of this code were successfully cross-checked with those obtained by other authors (Milne et al. 2004). This code was later generalized to three dimensions (Hirschmann 2009).

Before and around the epoch of maximum of the optical light curve, the γ -ray emission can be characterized (Fig. 2 of Gómez-Gomar et al. loc.cit.) as follows: i) a spectrum dominated by the ^{56}Ni 158 and 812 keV lines; ii) because of the rapid

expansion, the lines are blueshifted but their energy peak quickly evolves back to the red as matter becomes more and more transparent. The emergent lines are broad, typically from 3% to 5%. Because of the Doppler effect the 812 keV line blends with the quickly growing ^{56}Co 847 keV line, forming a broad feature; iii) the intensity of the ^{56}Ni lines rises very quickly with time, after being very weak at the beginning, even in the case of SCh models. This fact, together with the relatively short lifetime of ^{56}Ni , makes the observational window rather short.

SN 2011fe (RA = 14:03:05.81, Dec = +54:16:25.4; J2000) was discovered by M101 on August 24, 2011 (Nugent et al. 2011a). The absence of hydrogen and helium, coupled with the presence of silicon in the spectrum, clearly indicates that it belongs to the SNIa class. Since it was not visible on August 23, this supernova must have been detected about one day after the explosion (Nugent et al. 2011a). Furthermore, since M101 is at a distance of 6.4 Mpc (Stetson et al. 1998; Shappee & Stanek 2011), SN2011fe is the brightest SNIa detected in the last 25 years. This distance is slightly less than the maximum distance at which current gamma-ray instruments should be able to detect an intrinsically luminous SNIa. The closeness of SN2011fe has made it possible to obtain the tightest constraints on the supernova and its progenitor system to date in a variety of observational windows. Red giant and helium star companions, symbiotic systems, systems at the origin of optically thick winds or containing recurrent novae are excluded for SN2011fe (Li et al. 2011a; Bloom et al. 2012; Brown et al. 2012; Chomiuk et al. 2012), leaving only either DD or a few cases of SD as possible progenitor systems of this supernova.

In this study we analyze the data obtained by INTEGRAL during the optical pre-maximum observations spanning from 4258.8733 IJD (August 29, 20:59 UT) to 4272.1197 IJD (September 12, 2:52 UT) with a total observation time of 975 419 s. This schedule was essentially determined by the constraints imposed by the Sun, according to the TVP tool of INTEGRAL, which prevented the observation just beyond the optical maximum where the ^{56}Ni lines are expected to peak. Despite this limitation, these early observations were triggered to constrain any predicted early gamma-ray emission as may be expected from some variants of SCh models. In the next section, we present the data obtained with the instruments onboard INTEGRAL. Then, we discuss the limits they can put on present models of SNIa explosion and conclude.

2. INTEGRAL data

INTEGRAL (Winkler et al. 2003) is able to observe in gamma-rays, X-rays and visible light. It was launched in October 17, 2002 and was injected into a highly eccentric orbit with a period of about three days in such a way that it spends most of its time well outside the radiation belts of the Earth. The spacecraft contains two main instruments, SPI, a germanium spectrometer for the energy range of 18 keV to 8 MeV with a spectral resolution of 2.2 keV at 1.33 MeV (Vedrenne et al. 2003), and IBIS, an imager able to provide an imaging resolution of 12 arcmin FWHM (Ubertini et al. 2003), which has a CdTe detector, ISGRI, able to provide spectral information of the continuum and broad lines in the range of 15 keV to 1 MeV (Lebrun et al. 2003). Other onboard instruments are an X-ray monitor, JEM-X, that works in the range of 3 to 35 keV (Lund et al. 2003), and an optical camera, OMC, able to operate in the visible band of the spectrum up to a magnitude of 18 (Mas-Hesse et al. 2003).

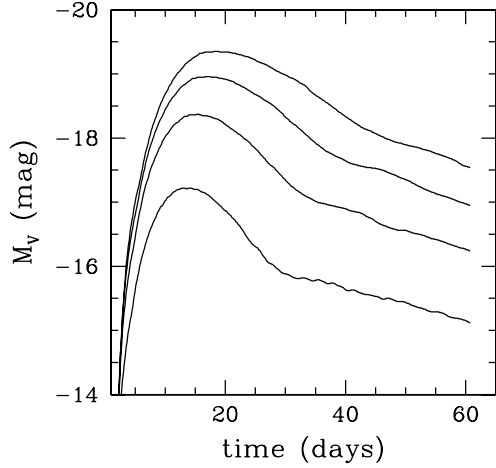


Fig. 1. Light curves in the V -band obtained from DDT models that produce, from top to bottom, 0.63, 0.45, 0.27, 0.09 M_{\odot} of ^{56}Ni and satisfy the brightness-decline relationship.

2.1. OMC data

The height of the maximum of the optical light curve depends on the total amount of ^{56}Ni synthesized during the explosion, its distribution in the debris, the total kinetic energy of matter and the opacity (Arnett 1996). The brightness decline relation (Δm_{15}) relates the absolute brightness at maximum light and the rate of the post-maximum decline over 15 days. This relationship is well understood from theory: light curves are powered by the radioactive decay of ^{56}Ni (Colgate & McKee 1969). More ^{56}Ni increases the luminosity and causes the envelopes to be hotter. Higher temperature means higher opacity, hence longer diffusion time scales and slower decline rates after maximum light (Hoefflich et al. 1996; Nugent et al. 1997; Umeda et al. 1999; Kasen et al. 2009). The Δm_{15} -relation holds up for virtually all explosion scenarios as long as there is an excess amount of stored energy to be released (Hoefflich et al. 1996; Baron et al. 2012). The tightness of the relation observed for Branch-normal SNe Ia is about 0.3^m (Hamuy et al. 1996; Perlmutter et al. 1999), and it is consistent with explosions of models of similar mass. Since DDT models (see Fig. 1) provide a reasonable spectral evolution, their maximum brightness is consistent with the Hubble constant and the Δm_{15} -relationship is consistent with the observations with a factor between 1 and 1.3, we use these models to estimate the total amount of ^{56}Ni freshly synthesized.

The properties and the photometric characterization of the OMC can be found in Mas-Hesse et al. (2003). The data obtained during the orbits 1084–1088 plus the data corresponding to orbits 1097–1111, were analyzed with the Offline Scientific Analysis Software (OSA, version 9) provided by the ISDC Data Centre for Astrophysics (Courvoisier et al. 2003). The fluxes and magnitudes were derived from a photometric aperture of 3×3 pixels (1 pixel = 17.504 arcsec), slightly circularized, i.e. removing one quarter pixel from each corner (standard output from OSA). The default centroiding algorithm was used, i.e. the photometric aperture was centered on the source coordinates. We checked that the photometric aperture of 3×3 pixels does not include any significant contribution by other objects. Because the source was bright enough, combining several shots was not required to increase the signal-to-noise ratio. To only include high-quality data, some selection criteria were applied to individual photometric points by removing those measurements with a problem flag. Shots were checked against saturation, rejecting

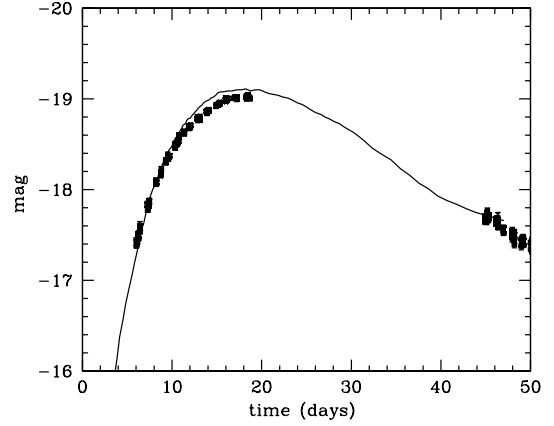


Fig. 2. Light curve of SN2011fe in the V -band obtained with the OMC/INTEGRAL assuming a distance of 6.4 Mpc (dots) for the orbits 1086–1088 and 1097–1101. The continuous line represents a reasonable fit obtained with a DDT model (see text).

those with long exposures (200 s) for $V < 10.5$. To avoid noisy measurements, the shortest exposures (10 s) were not used.

The extinction along the line of sight has two components, one due to the Milky Way and the other to M101. Since M101 has a galactic latitude of $\sim 60^\circ$ the Milky Way contribution is expected to be small. Shappee & Stanek (2011) estimate $E(B-V) = 0.009$ which means an extinction of $A_V \sim 0.03$ mag. The M101 contribution is also expected to be small since it is a face-on galaxy, and SN2011fe is placed in a region with a low concentration of interstellar dust and gas (Suzuki et al. 2007, 2009). It is possible to obtain a rough upper limit for the extinction using the observations (Shappee & Stanek 2011) of two regions containing Cepheids that overlap just at the position of SN2011fe. The average of the two extinctions, $E(B-V) = 0.2$ mag, would imply an absorption of $A_V = 0.62$ mag. However, since the region containing the supernova has a low concentration of interstellar matter, the comparison of the light curve at different bands and the absence of strong sodium lines in the spectrum suggest that extinction is small. Thus the adopted absorption affecting the supernova is taken to be $A_V \sim 0.03$.

The V -band light curve reached the maximum, $V = 9.99$, at the day IJD = 4271.44, in agreement with Richmond & Smith (2012). When taking a canonical distance of 6.4 Mpc (see, however, Tammann & Reindl (2011)) and assuming no extinction, the absolute magnitude should be $M_V = -19.04$ at its maximum, thus indicating that the SN2011fe was a slightly dim average SNIa. The V -band light curve can be well fitted with a delayed detonation model (see Fig. 2) of a Chandrasekhar mass white dwarf igniting at $\rho_C = 2 \times 10^9$ g cm $^{-3}$, making the transition deflagration/detonation at $\rho_{tr} = 2.2 \times 10^7$ g cm $^{-3}$. This model produces 0.51 M_{\odot} of ^{56}Ni , although if extinction and distance uncertainties are taken into account, this value could easily be around ten percent larger (Höflich et al. 2002). A value that is also consistent with the estimations by Röpke et al. (2012) using an independent DDT model and a violent merger model, and it is roughly equivalent to the one obtained with model DDTe of Table 2. We note that this yield of ^{56}Ni is consistent with the value derived by Nugent et al. (2011b). From this theoretical model, $\Delta m_{15}(B) = 1.2 \pm 0.2$, in agreement with Tammann & Reindl (2011) but slightly less than the value found by Richmond & Smith (2012). The observation of the early light curve, 4 h (Bloom et al. 2012), and 11 h (Nugent et al. 2011b) after the explosion strongly supports the scenario based on the explosion of a C/O white dwarf.

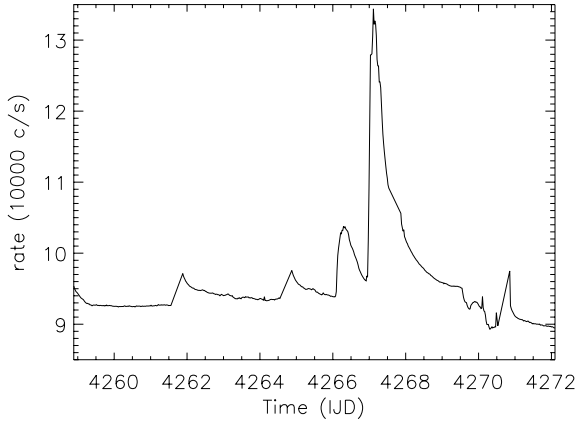


Fig. 3. Time variation of the event rate in the ACS of SPI during the pre-maximum observations of SN2011fe.

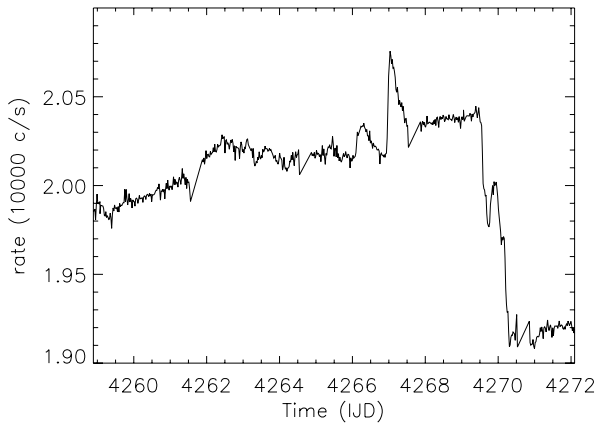


Fig. 4. Time variation of the event rate in the GeD of SPI during the pre-maximum observations of SN2011fe.

2.2. SPI data

Only data in the low-energy range (≤ 2 MeV) have been analyzed in this study of the SPI output. The energy calibration was performed for each orbit by fitting parameters of a four degree polynomial function with the channel positions of the instrumental background lines at 23.4 keV, 198.4 keV, 309.9 keV, 584.5 keV, 882.5 keV, and 1764.4 keV. The precision of the resulting calibration is better than ~ 0.1 keV at 1 MeV. The calibrated single-detector and multiple-detector¹ event data have been binned into separated spectra at 0.5 to 50 keV per bin.

The time-averaged energy spectrum of the supernova was extracted by a model fitting method. The flux of the source and the instrumental background are both fitted to the data (counts per detector per pointing at each energy bin), assuming a point source at the SN2011fe position. The instrumental background is fitted per pointing by assuming that the relative background rate in each detector of the Ge camera is fixed, and is obtained by summing the counts per detector of all the pointings of the observation. We have verified that the detector pattern did not change with time. This background modeling method is adapted to the analysis of data that show strong instrumental background

¹ We used only double-detector events because including events with greater detector multiplicity does not improve the sensitivity for this analysis (Attié et al. 2003).

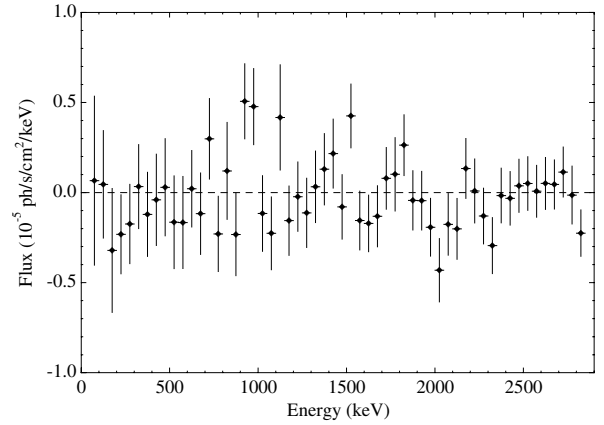


Fig. 5. Spectrum of the whole early observation of SN2011fe extracted from SPI data with 50 keV bins.

variations on time scales ≤ 3 days². Figures 3 and 4 display the count rate in the anticoincidence system (ACS) and in the germanium detector (GeD) of SPI. The ACS count rate could be used to trace the instrumental background fluctuations in the germanium detectors (Jean et al. 2003). The passage through the radiation belts and the impact of the solar activity are clearly seen. Solar activity was particularly influential during this period of observations because of two solar flares occurring on ~ 4266 and 4267 IJD followed by a Forbush decrease around 4268.5 IJD. To check that these background variations do not produce artifacts, we also performed the model-fitting analysis using a filtered data set without periods with strong rate variations. The results obtained with filtered and non-filtered data are statistically equivalent. Consequently, we decided to use unfiltered data in the next steps of the analysis.

Figure 5 displays the spectrum of the whole observation. It was obtained by combining the spectra extracted by model fitting from single-detector and multiple-detector events. In this case, the model fitting was performed with data rebinned in 50 keV bins. The spectrum does not show any significant feature. A χ^2 test shows that it is consistent with a Poissonian background ($\chi^2 = 12.4$ with a d.o.f. = 10). A similar conclusion is obtained when the spectra are extracted by model fitting with data rebinned in 5 keV or 2 keV bins.

No significant excess was found in the spectrum, even at the energies of the strongest gamma-ray lines that are expected from the decay of ^{56}Ni (blueshifted 158 and 812 keV lines). Table 1 presents the upper-limit fluxes derived from the analysis at the energies of interest for several band widths (Isern et al. 2011).

2.3. IBIS/ISGRI data

IBIS uses two detection layers to cover the same energy range as SPI. The low-energy camera, ISGRI, uses 16 384 thin CdTe detectors operated at ambient temperature. The imaging is much better ($12'$ FWHM) than for SPI, but the spectral resolution is more limited, and the efficiency begins to drop above 100 keV. As a result, the IBIS/ISGRI sensitivity to the 812 keV line from ^{56}Ni is far worse than the SPI one at the same energy even in the case of a broad line. Conversely, IBIS/ISGRI is much better at work than SPI to reveal a low-energy continuum or broad lines, such as the 158 keV ^{56}Ni or 122 keV ^{57}Co ones. To summarize

² The analyses performed with background models that use background tracers show strong systematics due to these large instrumental background variations.

Table 1. Upper limit of the flux in selected spectral regions for SPI (2σ), JEM-X (2σ), and IBIS/ISGRI (3σ) for the entire pre-maximum observation period.

Energy band (keV)	Upper-limit flux (photons $s^{-1} cm^{-2}$)	Instrument
3–10	5.0×10^{-4}	JEM-X
10–25	4.0×10^{-4}	JEM-X
3–25	1.0×10^{-3}	JEM-X
60–172	1.5×10^{-4}	IBIS/ISGRI
90–172	1.1×10^{-4}	IBIS/ISGRI
150–172	7.1×10^{-5}	IBIS/ISGRI
160–166	7.5×10^{-5}	SPI
140–175	2.3×10^{-4}	SPI
814–846	2.3×10^{-4}	SPI
800–900	3.5×10^{-4}	SPI

the picture, one could say that SPI is better at detecting narrow lines in a spectrum, while IBIS/ISGRI is better at detecting point sources in broad energy-range sky images. Two data processing methods have been followed in parallel. One uses the standard OSA-9 version and the other takes advantage of the developments for the forthcoming OSA-10. The latter approach includes two new corrections: for the spectral drift along the mission and for the flat field. In either case no significant (greater than 3σ) signal was found at the position of SN2011fe. Table 1 gives the upper limits obtained for the 60–170 keV, 90–172 keV and the 150–172 keV bands. Similarly, maps using the last six days of the observing period for the same energy ranges do not show any significant emission at the position of SN2011fe.

2.4. JEM-X data

Both JEM-X units were simultaneously operating at the time of these *INTEGRAL* observations and they can be used to constrain the continuum emission using a source search in broad band images as in the IBIS/ISGRI case. Owing to the smaller field of view of the JEM-X monitors compared to those of SPI and IBIS (Lund et al. 2003), we selected and analyzed only those pointings where SN2011fe was within 5° of the pointing direction. The data obtained during the orbits 1084–1088 (August 29 to September 12, 2011) were analyzed with OSA-9 following the standard procedure. Images from single pointings were combined into one mosaicked image for each X-ray monitor. The two composite images from JEM-X1 and JEM-X2 were then merged to obtain the final image, providing an on-source effective exposure time of 450 ks. The imaging analysis was performed in the 3–25 keV band, and in the 3–10 keV and 10–25 keV sub-bands. SN2011fe is not detected in any of the JEM-X images. Assuming a Crab-like spectrum, we estimate 2σ upper limits on the 3–10 keV and 10–25 keV fluxes of $5 \times 10^{-4} \text{ ph cm}^{-2} \text{ s}^{-1}$ and $4 \times 10^{-4} \text{ ph cm}^{-2} \text{ s}^{-1}$, respectively (see Table 1). The source is also not detected when analyzing the JEM-X data separately from orbits 1086–1088 (Sept 4th to 12th, 2011), corresponding to the observations closer to the epoch of the expected ^{56}Ni line maximum.

3. Discussion

The γ -ray spectrum of SNIa mainly depends on the total amount and distribution of ^{56}Ni synthesized during the explosion, as well as on the chemical structure and velocity distribution of the debris (Gómez-Gomar et al. 1998). For instance, when ^{56}Ni

Table 2. Kinetic energy (K) and mass of ^{56}Ni produced by different models of explosion.

Model	K (foe)	M_{Ni} (M_\odot)
DETO	1.44	1.16
DD202c	1.30	0.78
DDTc	1.16	0.74
SC3F	1.17	0.69
W7	1.24	0.59
SCOP3D	1.17	0.56
DDTe	1.09	0.51
SC1F	1.04	0.43
HED6	0.72	0.26

is present in the outer layers of some of the SCh models, the corresponding lines should appear very early in the spectrum. However, for a given flux, there are at least two more factors that determine whether the γ -signal is detectable: the change in the signal with time and the width of the lines.

To check the influence of the mass and distribution of ^{56}Ni , several models obtained under different hypotheses about the burning regime or the explosion mechanism have been considered. Most are one-dimensional, spherically symmetric models, which should be sufficient for SN2011fe in view of the small amount of global asymmetry suggested by spectropolarimetric measurements (Smith et al. 2011). We have not included models of DD explosions for two reasons. First, Nugent et al. (2011b) satisfactorily reduced the rising part of the light curve of SN2011fe with a simple analytic model involving a Chandrasekhar mass white dwarf, and found only small amounts of unburned carbon in the early spectra of this supernova. Second, in spite of recent advances on simulations of almost normal SNIa from mergers of massive white dwarfs (Pakmor et al. 2012), theoretical models of DD explosions are not as mature at present as those involving either Chandrasekhar or sub-Chandrasekhar mass white dwarfs accreting from a non-degenerate companion. The number of free parameters involved in DD explosions is therefore too large to allow for efficient constraints derived from upper limits on the gamma-ray emission of SN2011fe.

Table 2 displays the main characteristics of the models used in the present study. The DETO model (Badenes et al. 2003) corresponds to a pure detonation of a white dwarf near the Chandrasekhar limit. It is also representative of the most massive models computed by Fink et al. (2010). The W7 is the classical model of Nomoto et al. (1984). The DD202c (Hoeflich et al. 1998) and the DDTc,e (Badenes et al. 2005) models are delayed detonation models that produce different amounts of ^{56}Ni and have different expansion energies. The HED6 model corresponds to the explosion of a $0.6 M_\odot$ C/O WD that has accreted $0.17 M_\odot$ of helium in Hoeflich & Khokhlov (1996), and SC1F and SC3F (E. Bravo, unpublished) are also SCh models equivalent to models 1 and 3 of Fink et al. (2010). Finally, the SCOP3D model is a three-dimensional SCh model that corresponds to model A of García-Senz et al. (1999).

Figure 6 displays the SPI 2σ upper limit spectrum obtained with 5 keV bins as, well as the gamma ray spectra predicted by several models for this early observation, assuming that the distance of SN2011fe is 6.4 Mpc. All the models are well below the upper-limit. The predicted intensity of the ^{56}Ni 158 keV, 270 keV, 480 keV, 750 keV, and 812 keV lines is larger for the detonation model (DETO) and the SCh models SCOP3D, SC3F, and SC1F, as expected. Since the spectral shape (width and centroid) and intensity change from one model to another,

Table 3. Measured and predicted flux in spectral regions where ^{56}Ni lines are expected to be as a function of models.

Model	Energy band (keV)	Measured flux (10^{-4} photons $\text{s}^{-1} \text{cm}^{-2}$)	Predicted flux (10^{-4} photons $\text{s}^{-1} \text{cm}^{-2}$)	Probability %
DETO	150–175	-0.20 ± 0.78	0.81	92.4
	265–295	-0.55 ± 0.85	0.48	
	482–508	0.13 ± 0.88	0.36	
	730–880	-1.01 ± 2.02	2.01	
SCOP3D	145–170	-0.50 ± 0.76	0.70	84.7
	267–297	-0.24 ± 0.86	0.36	
	482–508	0.13 ± 0.88	0.27	
	720–880	-0.75 ± 2.08	1.54	
SC3F	150–170	-0.03 ± 0.67	0.37	62.4
	253–283	-0.99 ± 0.85	0.25	
	452–508	0.38 ± 1.42	0.29	
	720–880	-0.75 ± 2.08	0.76	
SC1F	150–170	-0.03 ± 0.67	0.32	51.8
	254–288	-0.81 ± 0.90	0.22	
	458–509	0.01 ± 1.37	0.23	
	725–900	-1.02 ± 2.18	0.63	
HED6	159–169	-0.13 ± 0.49	0.08	21.3
	270–284	-0.98 ± 0.59	0.05	
	475–505	-0.27 ± 1.04	0.06	
	746–872	-0.13 ± 1.87	0.27	
DDTc	158–165	-0.10 ± 0.57	0.03	6.2
	270–282	-0.58 ± 0.76	0.02	
	480–498	-1.22 ± 1.00	0.02	
	740–880	1.28 ± 2.08	0.08	
W7	158–165	-0.34 ± 0.69	0.02	3.4
	270–282	-0.88 ± 0.92	0.02	
	478–498	-1.82 ± 1.37	0.02	
	740–880	-0.31 ± 1.38	0.04	
DDTe	158–165	-0.34 ± 0.69	0.01	2.0
	270–280	-0.49 ± 0.84	0.008	
	480–498	-1.00 ± 1.26	0.009	
	740–880	-0.152 ± 3.25	0.05	

Notes. The fifth column is the probability of rejecting the model (see text). In the case of DDTc, W7 and DDTe models, the fluxes were obtained for an optimal observation periods of 7, 5 and 5 days, respectively (see Table 4).

the energy band used to extract the fluxes of every line or complex of lines was chosen to provide the optimum significance for each model. Results are displayed in Table 3.

Despite this non-detection and the bounds imposed by the optical light curve, the compatibility of the different models with the zero flux hypothesis has been tested. Since the measured fluxes are compatible with zero, the χ^2 value for each model was computed as the quadratic sum of the expected significance of the predicted fluxes³. Then, the probability of rejection of each particular model was derived by computing the probability that the χ^2 is smaller than the measured value within χ^2 statistics. The rejection probability of the selected models is given in the fifth column of Table 3. None of them can be firmly rejected by SPI data. Although the probability of rejecting the DETO model is 92.4%, this value corresponds to a significance of $\sim 1.4\sigma$. To reject it at a 99% of confidence level, the intensity of the lines should be higher by a factor 1.45 times or, equivalently, the distance to SN2011fe should be less than 5.3 Mpc. Since the DETO model is the one that produces the brightest lines, SPI can only provide interesting results during this epoch if the distance to the supernova is less than this value.

The influence of the temporal behavior of the line intensity and line width on the detectability of the γ emission can be easily

seen by estimating the significance of the observation. In the limit of weak signals this significance is given by (Jean 1996)

$$n_\sigma = \frac{A_{\text{eff}} \int_{t_i - \Delta t}^{t_i} \varphi(t) dt}{\sqrt{bV\Delta E\Delta t}} \quad (1)$$

where Δt is the observation time, A_{eff} the effective area at the corresponding energies, φ is the flux ($\text{cm}^{-2} \text{s}^{-1}$) in the energy band ΔE , V is the volume of the detector, and b the specific noise rate ($\text{cm}^{-3} \text{s}^{-1} \text{keV}^{-1}$), where it has been assumed that it is weakly dependent on the energy and time in the interval of interest.

If the flux grows like $\varphi(t) = \varphi_0 e^{\alpha t}$, the significance reached by integrating the time interval $(t_i - \Delta t, t_i)$ is

$$n_\sigma = \frac{A_{\text{eff}} \varphi(t_i)}{\sqrt{abV\Delta E}} \frac{1 - e^{-\alpha\Delta t}}{\sqrt{\alpha\Delta t}} \quad (2)$$

For $\alpha\Delta t \ll 1$, the significance behaves as $n_\sigma \propto \sqrt{\Delta t}$ and has a maximum at $\alpha\Delta t = 1.26$. Furthermore, the dependence on ΔE clearly shows the convenience of taking a value that maximizes the signal to noise ratio. Unfortunately, since the value of α is not known a priori, the optimal observing time is not known in advance. Since the time dependence of the model fluxes does not strictly follow an exponential growth, we analyzed the optimum

³ The expected significance is the predicted flux divided by the uncertainty of the flux measurement in the corresponding energy band.

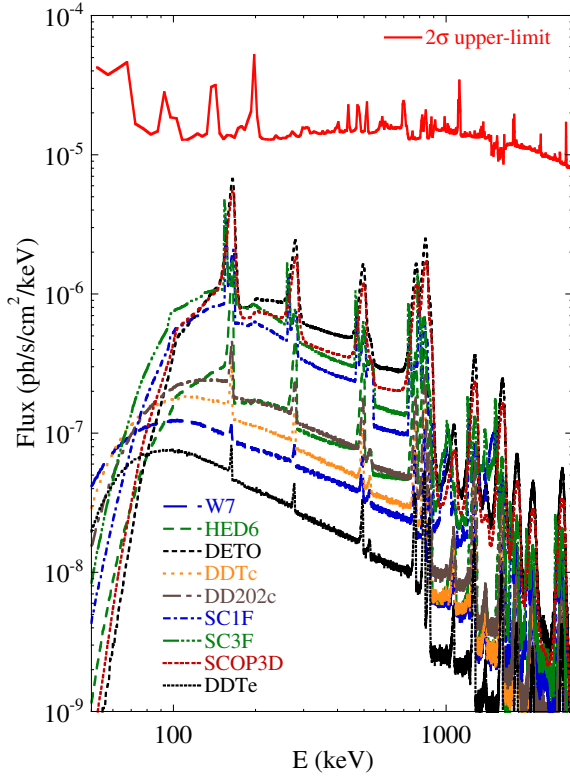


Fig. 6. Comparison of the mean flux obtained from the theoretical models during the early observation period with the 2σ upper-limit flux in 5 keV bins. Theoretical spectra were obtained with the code described in Gómez-Gomar et al. (1998).

observation periods for each model. Table 4 displays the results. In general, models and energy ranges showing weak variation of the flux are best detected when the observation period is long whereas models with a strong variation in their flux during the first two weeks are best detected using data at those times.

It is well known (Gómez-Gomar et al. 1998) that the width of the line has a strong influence on their detectability. In the case of the present observations it is possible to estimate the significance of a narrow line, $\Delta E \lesssim 2$ keV, by comparing the measured 1σ flux uncertainty (see Table 3), φ_1 , with the flux φ and the width ΔE predicted by the model

$$n_\sigma \approx \frac{\varphi}{\varphi_1} \sqrt{\frac{\Delta E}{2 \text{ keV}}}. \quad (3)$$

In the case of the 158 keV line (Table 3), the flux predicted by the DETO model is $\varphi = 8.1 \times 10^{-5} \text{ ph s}^{-1} \text{ cm}^{-2}$, $\varphi_1 = 7.8 \times 10^{-5} \text{ ph s}^{-1} \text{ cm}^{-2}$, and $\Delta E = 25$ keV, where ΔE has been chosen to maximize the signal to noise ratio. With these data, $n \sim 3.8$, and in this case with this hypothesis, the 158 keV line would have been detected by SPI if it had been narrow. In contrast, in the model SC1F, $\varphi = 3.2 \times 10^{-5} \text{ ph s}^{-1} \text{ cm}^{-2}$, $\varphi_1 = 6.7 \times 10^{-5} \text{ ph s}^{-1} \text{ cm}^{-2}$, $\Delta E = 20$ keV and the result is $n \sim 1.5$. Here, the line would only be marginally detectable even in the narrow case.

The luminosity at the maximum of the optical light curve is proportional to the total mass of ^{56}Ni , while the shape of the optical peak is determined by the amount of ^{56}Ni and the kinetic energy of the remnant (Arnett 1997). As already been mentioned, the favored model by the optical light curve is the DDTe one, and it seems worthwhile to interpret the SPI observations in terms of this model.

Table 4. Optimal observation period for several models and energy ranges with SPI.

Model	Energy band (keV)	Optimal period (days)
DETO	150–175	13.5
	730–880	13.5
SCOP3D	145–170	13.5
	750–880	13.5
SC1F	150–170	13.4
	725–900	13.4
HED6	155–175	11.7
	730–880	12.4
DDTc	70–165	8.0
	740–880	6.2
W7	70–900	5.7
	820–840	4.7
DDTe	158–165	4.9
	740–880	4.9

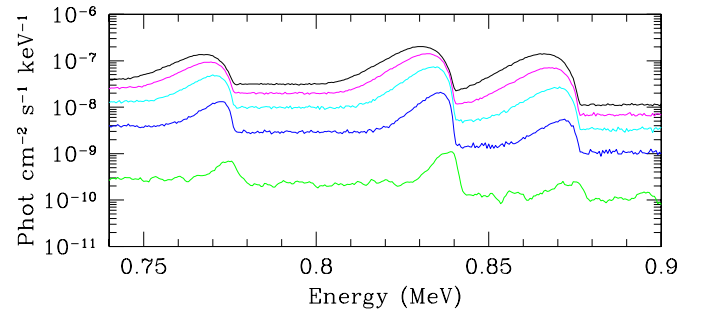
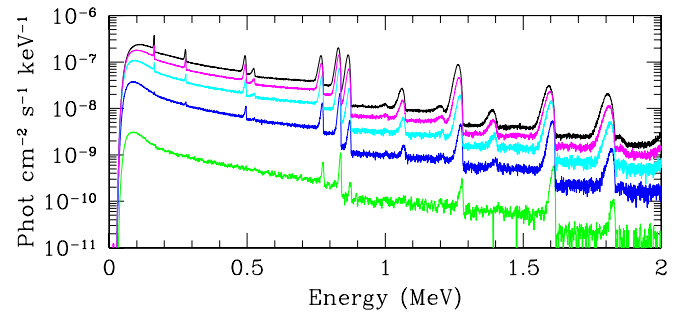


Fig. 7. Early gamma ray spectra predicted by the delayed detonation model that best fits the OMC (see Fig. 2) at days 8, 11, 14, 17, 20 (green, blue, cyan, magenta, black) at a distance of 6.4 Mpc (*upper figure*). The *lower panel* displays the evolution of the profile of the ^{56}Ni 812 keV- ^{56}Co 847 keV features.

Figure 7 (upper panel) displays the early gamma ray spectra predicted by DDTe for several instants after the explosion. The way the different lines grow and the width of them is clearly seen. The main problem with the 812 keV line is that, owing to the Doppler effect and energy degradation of photons by Compton scattering, it blends with the 847 keV line of ^{56}Co (see Fig. 7, lower panel) and makes it more difficult to interpret the signal. During this observation, and for this model, the energy interval that maximizes the signal to noise ratio is ~ 25 keV centered at 826 keV, and the corresponding flux at day 18 is $\varphi = 3.4 \times 10^{-6} \text{ ph s}^{-1} \text{ cm}^{-2}$. In contrast, the 158 keV line has a more regular behavior and it is better suited to diagnostic purposes. At day 20 after the explosion, the flux in this line is $\varphi = 4.7 \times 10^{-6} \text{ ph s}^{-1} \text{ cm}^{-2}$ for $\Delta E = 20$ keV. In both cases, the signal is too weak to be detected with SPI, and the source should be at a distance of $\lesssim 2$ Mpc to be detectable.

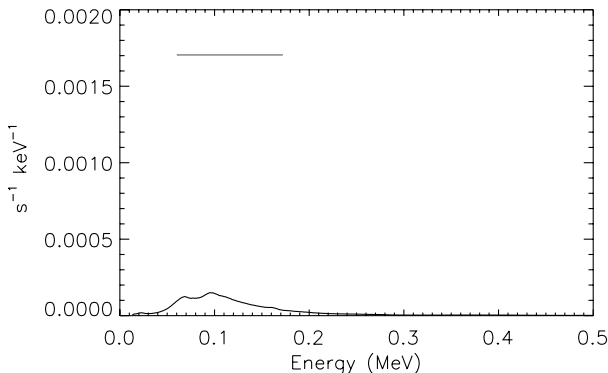


Fig. 8. ISGRI expected rate spectrum from a DDTe model averaged over the last 6 days of the first observation period. The 3σ ISGRI upper limit for the 60–172 keV band is displayed as a horizontal bar.

The 200–540 keV band contains almost all the photons produced by the annihilation of positrons produced during the ^{56}Ni chain decay. Since the emission of 511 keV only represents the 25% of the total number of the annihilation photons, this band offers, in principle, better possibilities of detection than the 511 keV line itself. In the DDTe model, the maximum of the band occurs at day 50 and amounts of $1.05 \times 10^{-4} \text{ ph s}^{-1} \text{ cm}^{-2}$, while the maximum of the 511 keV line occurs at day 74 with a flux of $1.2 \times 10^{-5} \text{ ph s}^{-1} \text{ cm}^{-2}$, within a band of 30 keV. The expected emission at day 18 after the explosion, the last day of this observation window, are $4.9 \times 10^{-5} \text{ ph s}^{-1} \text{ cm}^{-2}$ and $2.4 \times 10^{-6} \text{ ph s}^{-1} \text{ cm}^{-2}$. The 3σ sensitivity in this band is estimated to be $8.7 \times 10^{-4} \text{ ph s}^{-1} \text{ cm}^{-2}$ for an integration time of 10^6 s , well above the value of the expected emission for this model, for which reason this band is not detectable by SPI/INTEGRAL except if the explosion occurs at a distance $d \lesssim 1\text{--}2 \text{ Mpc}$ (assuming an explosion similar to what is predicted by the DDTe model).

As in the case of SPI, it is possible to discuss the results from ISGRI in more depth using detailed predictions by different theoretical models. In this case we use the model to produce a daily spectrum corresponding to the period of observation and combine these spectra with the ISGRI sensitive area (ARF) and spectral response (RMF) to predict the observable ISGRI spectrum as a function of time. Using the latest ISGRI background estimate (Mattana, priv. comm.), the expected relative value of the signal-to-noise ratio can be computed as a function of energy and time. This was done for the DDTe, W7, DETO, and SC3F models. The first two of these models predict fluxes that are out of the reach of the ISGRI sensitivity by an order of magnitude even if only the last days of the observing period are used, where the expected signal is higher. Figure 8 illustrates an attempt in the case of the DDTe model. The 60–172 keV upper limit on the ISGRI rate during the last six days of the first observation period is $1.7 \times 10^{-3} \text{ s}^{-1} \text{ keV}^{-1}$, which represents $2.2 \times 10^{-4} \text{ cm}^{-2} \text{ s}^{-1}$.

Since the DETO and SC3F models produce important amounts of ^{56}Ni near the surface, they display an important emission feature in the $\sim 150\text{--}170 \text{ keV}$ band. Figure 9 displays the spectrum that could be expected from the DETO model. This spectrum is an average over all the time that ISGRI has been pointed at the source and the optimal band corresponds to 150–172 keV. In this case the 3σ limit corresponds to $7.1 \times 10^{-5} \text{ cm}^{-2} \text{ s}^{-1}$. If a source like DETO were been present, the significance of the signal would have been 2.8σ , but there was nothing detected by ISGRI in the field. Model SC3F exhibits similar behavior (Fig. 10), and for the same specifications, the

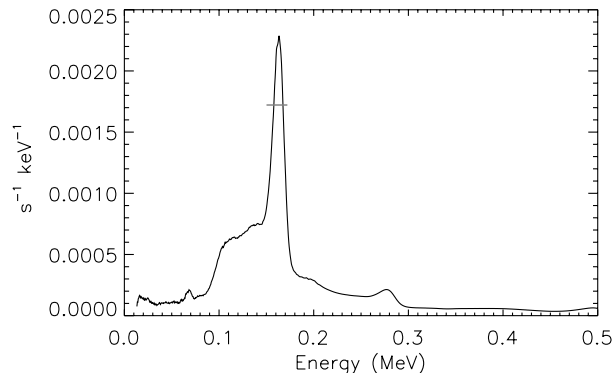


Fig. 9. ISGRI expected rate spectrum from a DETO model averaged over the entire observation period. The 3σ ISGRI upper limit for the 150–172 keV band is displayed as a horizontal bar.

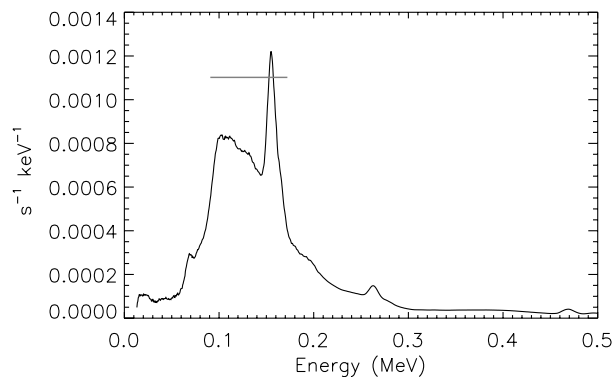


Fig. 10. ISGRI expected rate spectrum from an SC3F model averaged over the entire observation period. The 3σ ISGRI upper limit for the 90–172 keV band is displayed as a horizontal bar.

significance in the band is 1.4σ . However, in this case, the continuous emission at low energies is important and the optimal observation band is 90–172 keV, while the 3σ limit is $1.1 \times 10^{-4} \text{ cm}^{-2} \text{ s}^{-1}$ and the significance of the signal would have been 2.1σ . If these models, which synthesize 1.16 and $0.69 M_{\odot}$ of ^{56}Ni , respectively, are scaled to the $\sim 0.5 M_{\odot}$ demanded by the observations of SN2011fe in the optical, their expected gamma-ray flux would be marginally above the ISGRI sensitivity limit.

4. Conclusions

SN2011fe was observed with the four instruments SPI, ISGRI/IBIS, JEM-X, and OMC operating onboard INTEGRAL just before the maximum of the optical light curve for a period of time of 1000 ks, and the data were compared with the predictions of several theoretical models. SPI data in the bands containing the 158 keV and the 812 keV emission of ^{56}Ni would have allowed us to reject at 98% confidence level (2σ) models that produce large amounts of ^{56}Ni near the surface, if the supernova were closer. For instance, models with a mass fraction of ^{56}Ni in the outer $0.15 M_{\odot}$ of 0.05 and 0.5 would have been rejected if the supernova distance was closer than 1.4 and 3.7 Mpc respectively, assuming non-detection. Furthermore, ISGRI/IBIS has proved to be very efficient at exploring the low-energy region ($\sim 100 \text{ keV}$) and has confirmed that there were not significant amounts of radioactive elements in the outer layers. This picture is consistent with the light curve obtained with the OMC. The observations in the optical suggest that the total amount of ^{56}Ni produced in the event is $\sim 0.5 M_{\odot}$ triggered by a mild DDT explosion.

Acknowledgements. This work was supported by the MINECO-FEDER grants AYA08-1839/ESP, AYA2011-24704/ESP, AYA2011-24780/ESP, AYA2009-14648-C02-01, CONSOLIDER CSC2007-00050, by the ESF EUROCORES Program EuroGENESIS (MINECO grants EUI2009-04170), by the grant 2009SGR315 of the Generalitat de Catalunya. In parts, this work was also supported by the NSF grants AST-0708855 and AST-1008962 to PAH. The INTEGRAL SPI project was completed under the responsibility and leadership of the CNES. We also acknowledge the INTEGRAL Project Scientist Chris Winkler (ESA, ESTEC) and the INTEGRAL personnel for their support of these observations.

References

- Ambwani, K., & Sutherland, P. 1988, *ApJ*, 325, 820
- Arnett, D. 1996, *Supernovae and Nucleosynthesis* (Princeton: University Press)
- Arnett, D. 1997, in *Thermonuclear Supernovae*, eds. P. Ruiz-Lapuente, R. Canal, & J. Isern, NATO ASIC Proc., 486, 405
- Attié, D., Cordier, B., Gros, M., et al. 2003, *A&A*, 411, L71
- Badenes, C., Bravo, E., Borkowski, K. J., & Domínguez, I. 2003, *ApJ*, 593, 358
- Badenes, C., Borkowski, K. J., & Bravo, E. 2005, *ApJ*, 624, 198
- Baron, E., Höflich, P., Krisciunas, K., et al. 2012, *ApJ*, 753, 105
- Bloom, J. S., Kasen, D., Shen, K. J., et al. 2012, *ApJ*, 744, L17
- Brown, P. J., Dawson, K. S., & Pasquale, M., et al. 2012, *ApJ*, 753, 22
- Burrows, A., & The, L.-S. 1990, *ApJ*, 360, 626
- Chomiuk, L., Soderberg, A. M., Moe, M., et al. 2012, *ApJ*, 750, 164
- Colgate, S. A., & McKee, C. 1969, *ApJ*, 157, 623
- Courvoisier, T. J.-L., Walter, R., Beckmann, V., et al. 2003, *A&A*, 411, L53
- Edwards, Z. I., Pagnotta, A., & Schaefer, B. E. 2012, *ApJ*, 747, L19
- Fink, M., Röpke, F. K., Hillebrandt, W., et al. 2010, *A&A*, 514, A53
- García-Senz, D., Bravo, E., & Woosley, S. E. 1999, *A&A*, 349, 177
- Gehrels, N., Leventhal, M., & MacCallum, C. J. 1987, *ApJ*, 322, 215
- Georgii, R., Plüschke, S., Diehl, R., et al. 2002, *A&A*, 394, 517
- Gómez-Gomar, J., Isern, J., & Jean, P. 1998, *MNRAS*, 295, 1
- González Hernández, J. I., Ruiz-Lapuente, P., Filippenko, A. V., et al. 2009, *ApJ*, 691, 1
- Hamuy, M., Phillips, M. M., Suntzeff, N. B., et al. 1996, *AJ*, 112, 2408
- Hillebrandt, W., & Niemeyer, J. C. 2000, *ARA&A*, 38, 191
- Hirschmann, A. 2009, Ph.D. Thesis, Universitat Politècnica de Catalunya (UPC) – Institut d'Estudis Espacials de Catalunya (IEEC)
- Höflich, P., & Khokhlov, A. 1996, *ApJ*, 457, 500
- Höflich, P., Khokhlov, A., & Mueller, E. 1994, *ApJS*, 92, 501
- Höflich, P., Khokhlov, A., Wheeler, J. C., et al. 1996, *ApJ*, 472, L81
- Höflich, P., Wheeler, J. C., & Thielemann, F. K. 1998, *ApJ*, 495, 617
- Höflich, P., Gerardy, C. L., Fesen, R. A., & Sakai, S. 2002, *ApJ*, 568, 791
- Hoyle, F., & Fowler, W. A. 1960, *ApJ*, 132, 565
- Iben, Jr., I., & Tutukov, A. V. 1985, *ApJS*, 58, 661
- Isern, J., Bravo, E., & Hirschmann, A. 2008, *New Astron. Rev.*, 52, 377
- Isern, J., Jean, P., Bravo, E., et al. 2011, *ATel*, 3683, 1
- Jean, P. 1996, Ph.D. Thesis, Université Paul Sabatier, Toulouse
- Jean, P., Vedrenne, G., Roques, J. P., et al. 2003, *A&A*, 411, L107
- Kasen, D., Röpke, F. K., & Woosley, S. E. 2009, *Nature*, 460, 869
- Kerzendorf, W. E., Schmidt, B. P., Asplund, M., et al. 2009, *ApJ*, 701, 1665
- Kumagai, S., & Nomoto, K. 1997, in *Thermonuclear Supernovae*, eds. P. Ruiz-Lapuente, R. Canal, & J. Isern, NATO ASIC Proc., 486, 515
- Lebrun, F., Leray, J. P., Lavocat, P., et al. 2003, *A&A*, 411, L141
- Lí, W., Bloom, J. S., Podsiadlowski, P., et al. 2011a, *Nature*, 480, 348
- Lí, W., Chornock, R., Leaman, J., et al. 2011b, *MNRAS*, 412, 1473
- Lí, W., Leaman, J., Chornock, R., et al. 2011c, *MNRAS*, 412, 1441
- Lichti, G. G., Bennett, K., den Herder, J. W., et al. 1994, *A&A*, 292, 569
- Lund, N., Budtz-Jørgensen, C., Westergaard, N. J., et al. 2003, *A&A*, 411, L231
- Mas-Hesse, J. M., Giménez, A., Culhane, J. L., et al. 2003, *A&A*, 411, L261
- Milne, P. A., Hungerford, A. L., Fryer, C. L., et al. 2004, *ApJ*, 613, 1101
- Nomoto, K., Thielemann, F.-K., & Yokoi, K. 1984, *ApJ*, 286, 644
- Nugent, P., Baron, E., Branch, D., Fisher, A., & Hauschildt, P. H. 1997, *ApJ*, 485, 812
- Nugent, P., Sullivan, M., Bersier, D., et al. 2011a, *ATel*, 3581, 1
- Nugent, P. E., Sullivan, M., Cenko, S. B., et al. 2011b, *Nature*, 480, 344
- Pakmor, R., Kromer, M., Taubenberger, S., et al. 2012, *ApJ*, 747, L10
- Perlmutter, S., Turner, M. S., & White, M. 1999, *Phys. Rev. Lett.*, 83, 670
- Pozdnyakov, L. A., Sobol, I. M., & Syunyaev, R. A. 1983, *Astrophys. Space Phys. Rev.*, 2, 189
- Richmond, M. W., & Smith, H. A. 2012, *The Journal of the American Association of Variable Star Observers*, 40, 872
- Röpke, F. K., Kromer, M., Seitenzahl, I. R., et al. 2012, *ApJ*, 750, L19
- Ruiz-Lapuente, P., Lichti, G. G., Lehoucq, R., Canal, R., & Casse, M. 1993, *ApJ*, 417, 547
- Ruiz-Lapuente, P., Comeron, F., Méndez, J., et al. 2004, *Nature*, 431, 1069
- Schaefer, B. E., & Pagnotta, A. 2012, *Nature*, 481, 164
- Shappee, B. J., & Stanek, K. Z. 2011, *ApJ*, 733, 124
- Sim, S. A., & Mazzali, P. A. 2008, *MNRAS*, 385, 1681
- Smith, P. S., Williams, G. G., Smith, N., et al. 2011 [[arXiv:1111.6626](https://arxiv.org/abs/1111.6626)]
- Stetson, P. B., Saha, A., Ferrarese, L., et al. 1998, *ApJ*, 508, 491
- Suzuki, T., Kaneda, H., Nakagawa, T., Makiuti, S., & Okada, Y. 2007, *PASJ*, 59, 473
- Suzuki, T., Kaneda, H., Onaka, T., Nakagawa, T., & Shibai, H. 2009, in *AKARI, a Light to Illuminate the Misty Universe*, eds. T. Onaka, G. J. White, T. Nakagawa, & I. Yamamura, ASP Conf. Ser., 418, 487
- Tammann, G. A., & Reindl, B. 2011, *ApJ*, submitted [[arXiv:1112.0439](https://arxiv.org/abs/1112.0439)]
- Timmes, F. X., & Woosley, S. E. 1997, *ApJ*, 489, 160
- Ubertini, P., Lebrun, F., Di Cocco, G., et al. 2003, *A&A*, 411, L131
- Umeda, H., Nomoto, K., Kobayashi, C., Hachisu, I., & Kato, M. 1999, *ApJ*, 522, L43
- Vedrenne, G., Roques, J.-P., Schönfelder, V., et al. 2003, *A&A*, 411, L63
- Webbink, R. F. 1984, *ApJ*, 277, 355
- Whelan, J., & Iben, Jr., I. 1973, *ApJ*, 186, 1007
- Winkler, C., Courvoisier, T. J.-L., Di Cocco, G., et al. 2003, *A&A*, 411, L1
- Woosley, S. E., & Kasen, D. 2011, *ApJ*, 734, 38

¹ Institut de Ciències de l'Espai (ICE-CSIC/IEEC), Campus UAB, 08193 Bellaterra, Barcelona, Spain

e-mail: [nelias;ieec.cat;hirschmann;isern;kulebi]@ieec.cat

² Université de Toulouse, UPS-OMP, IRAP, 31000 Toulouse, France

³ IRAP, 9 Av. colonel Roche, BP44346, 31028 Toulouse Cedex 4, France

e-mail: [pierre.jean;jknodlsede]@irap.omp.eu;

[pvb;vedrenne]@cesr.fr

⁴ Dept. Física i Enginyeria Nuclear, Univ. Politècnica de Catalunya, 08005 Barcelona, Spain

e-mail: [eduardo.bravo;domingo.garcia]@upc.edu

⁵ Max Planck Institut for Extraterrestrial Physics, Giessenbachstrasse 1, 85741 Garching, Germany

e-mail: [rod;grl;zhangx]@mpe.mpg.de

⁶ Centro de Astrobiología (CAB-CSIC/INTA), PO Box 78, 28691 Villanueva de la Cañada, Madrid, Spain

e-mail: albert@cab.inta-csic.es

⁷ Physics Department, Florida State University, Tallahassee, FL 32306, USA

e-mail: pah@astro.physics.fsu.edu

⁸ AstroParticule et Cosmologie (APC), CNRS-UMR 7164, Université de Paris 7 Denis Diderot, 75205 Paris, France

e-mail: lebrun@apc.univ-paris7.fr

⁹ Laboratoire Univers et Particules de Montpellier (LUPM), UMR 5299, Université de Montpellier II, 34095 Montpellier, France

e-mail: mrenaud@lupm.univ-montp2.fr

¹⁰ AIM (UMR 7158 CEA/DSM-CNRS-Université Paris Diderot), Irfu/Service d'Astrophysique, 91191 Gif-sur-Yvette, France

e-mail: simona.soldi@cea.fr

¹¹ Department of Physics and Astronomy & Pittsburgh Particle Physics, Astrophysics and Cosmology Center (PITT-PACC), University of Pittsburgh, Pittsburgh PA15260, USA

e-mail: badenes@pitt.edu

¹² Universidad de Granada, C/Bajo de Hueter 24, Apdo 3004, 180719, Granada, Spain

e-mail: inma@ugr.es

¹³ Dept. d'Astronomia i Meteorologia, Institut de Ciències del Cosmos (ICC), Universitat de Barcelona (IEEC-UB), 08014 Barcelona, Spain

e-mail: carme.jordi@ub.edu